Distributed Energy Management for Community Microgrids Considering Network Operational Constraints and Building Thermal Dynamics

Guodong Liu[a], Tao Jiang[b,*], Thomas B. Ollis[a], Xiaohu Zhang[c], Kevin Tomsovic[d]

[a] *Power and Energy Systems Group, Oak Ridge National Laboratory, One Bethel Valley Road, P.O. Box 2008, MS-6007, Oak Ridge, TN 37831-6007, USA*

[b] *Department of Electrical Engineering, Northeast Electric Power University, No.169 Changchun Road, Jilin 132012, China*

[c] *Global Energy Interconnection Research Institute North America (GEIRINA), 250 W. Tasman Dr., San Jose, CA 95134, USA*

[d] *Department of Electrical Engineering and Computer Science, The University of Tennessee, Knoxville, 1520 Middle Dr., Knoxville, TN 37996, USA*

Abstract

A distributed energy management system for community microgrids is developed in this paper. Unlike a centralized optimization-based energy management system, it schedules distributed energy resources and energy storage systems, as well as residential appliances, indirectly through iterative interaction between the microgrid central controller and home energy management systems, based on price signals. In each iteration, the microgrid central controller adjusts the scheduling of distributed energy resources and energy storage systems at the microgrid level. Meanwhile, the home energy management system of each house adjusts the scheduling of residential appliances. Then, the energy price at each bus is updated according to the unbalanced power between generation and demand. The optimization converges when the unbalanced power of all buses is close to zero, i.e., the microgrid central controller and home energy management systems reach an agreement on the energy price and generation/consumption. In particular, a detailed thermal dynamic model of the house is integrated into the HEMS scheduling for intelligent control of the heating, ventilation, and air-conditioning system by customers. The distribution network is also considered to make the energy price signal locational. Results of case studies validate the efficacy of the proposed distributed energy management system.

Keywords: Distributed optimization, community microgrids, energy management,

*Corresponding author. Tel.: +86 15022740069; fax.: +86 432 64806691.

Email addresses: liug@ornl.gov (Guodong Liu), tjiang@neepu.edu.cn (Tao Jiang), ollistb@ornl.gov (Thomas B. Ollis), xiaohu.zhang@geirina.net (Xiaohu Zhang), tomsovic@utk.edu (Kevin Tomsovic)

distribution network, building thermal dynamics.

Nomenclature

The symbols used in this paper are defined below. The term (k) in the upper right position stands for the value of the symbol's k-th iteration. A bold symbol stands for its corresponding vector.

0.1. Indices and Sets

b	Index of ESSs, running from 1 to N_B.
f	Index of feeders, running from 1 to N_F.
h	Index of houses, running from 1 to N_H.
g	Index of DGs, running from 1 to N_G.
k	Index of iterations,running from 1 to N_K.
m	Index of energy blocks offered by DGs, running from 1 to N_I.
n	Index of buses, running from 1 to N_N.
t	Index of time periods, running from 1 to N_T.
v	Index of PV generation, running from 1 to N_V.
$\mathcal{G}_n, \mathcal{B}_n, \mathcal{H}_n, \mathcal{V}_n$	Sets of DGs, ESSs, houses and PV connected at bus n.
Ω	Sets of feeders.

0.2. Variables

0.2.1. Binary Variables

u_{gt}	1 if DG g is on during period t and 0 otherwise.
$u_{ht}^{\mathrm{C}}, u_{ht}^{\mathrm{H}}$	1 if HVAC of house h is scheduled for cooling/heating during period t and 0 otherwise.
$u_{bt}^{\mathrm{C}}, u_{bt}^{\mathrm{D}}$	1 if battery b is scheduled for charging/discharging during period t and 0 otherwise.

0.2.2. Continuous Variables

l_{ft} Squared amplitudes of current on line f at t (A^2).

$p_{gt}(m)$ Power output scheduled from the m-th block of energy offer by DG g during period t (kW).

P_{ft}, Q_{ft} Real/reactive power flow on line f at t (kW, kVar).

P_{gt}, Q_{gt} Real/reactive power output scheduled for DG g during period t (kW, kVar).

$P_{bt}^{\mathrm{C}}, P_{bt}^{\mathrm{D}}$ Charging/discharging power of ESS b at t (kW).

$P_t^{\mathrm{PCC}}, Q_t^{\mathrm{PCC}}$ Real/ reactive power of PCC at t (kW, kVar).

P_{ht}, Q_{ht} Real/reactive load of house h at t (kW, kVar).

$P_{ht}^{\mathrm{LS}}, Q_{ht}^{\mathrm{LS}}$ Voluntary load curtailment of real/reactive power in house h at period t (kW, kVar).

Q_{bt} Reactive power of ESS b during period t (kVar).

R_{nt} Generation and demand mismatch (primal residual) at bus n during period t (kW).

S_{nt} Dual Residual at bus n during period t (kW).

SOC_{bt} State of charge of ESS b during period t (kWh).

T_{ht}^{In} Indoor temperature of house h at period t (°C).

T_{ht}^{M} The temperature of thermal accumulating layer of inner walls and floor in house h at period t (°C).

T_{ht}^{E} The temperature of house envelop at period t (°C).

V_{nt} Voltage magnitude of bus n during period t (p.u.).

λ_{nt} Lagrange multiplier of power balance equation at bus n during period t ($/kWh).

0.3. Constants

A_h The effective window area of house h (m^2).

C_{bt} Degradation cost of ESS b at period t ($/kWh).

$C_h^{\mathrm{In}}, C_h^{\mathrm{M}}, C_h^{\mathrm{E}}$ Thermal capacitance of indoor air, inner walls and envelope of house h (°C/kW).

$I_f^{\max}$ Maximum amplitudes of current on line f (A).

$p_{gt}^{\max}(m)$ Maximum output scheduled from the m-th block of energy offer by DG g during period t (kW).

$P_g^{\max}, P_g^{\min}$ Maximum/minimum output of DG g (kW).

$P^{\mathrm{PCC,max}}$ Maximum input/output power at PCC (kW).

P_{vt}, Q_{vt} Power output from PV v at period t (kW, kVar).

$P_{ht}^{\mathrm{O}}, Q_{ht}^{\mathrm{O}}$ Non-HVAC real/reactive power consumption in house h during period t (kW, kVar).

P_h^H Rated power of HVAC system in house h (kW).

$P_b^{\mathrm{C,max}}, P_b^{\mathrm{D,max}}$ Maximum charging/discharging power of ESS b (kW).

p_h^s The fraction of the general irradiance of the building's surroundings absorbed by the inner walls and floor of house h. The rest of the irradiance is absorbed by the indoor air.

r_f, x_f resistance and reactance of line f (Ω).

$R_h^{\mathrm{A}}, R_h^{\mathrm{E}}, R_h^{\mathrm{EA}}$ Thermal resistance between indoor air and ambient, indoor air and house envelope, house envelope and ambient of house h (°C/kW).

R_h^{M} Thermal resistance between indoor air and the thermal accumulating layer in the inner walls and floor of house h (°C/kW).

$R^{\max}$ Maximum primal residual for convergence (kW).

$S^{\max}$ Maximum dual residual for convergence (kW).

S_g, S_b Apparent power limit of DG g and ESS b (kVA).

$SOC_{bt}^{\max}, SOC_{bt}^{\min}$ Maximum/minimum state of charge of ESS b during period t (kWh).

T_t^{A} Ambient temperature as a combination of outside temperature and solar irradiance on residential building outer wall during period t (°C).

T_{ht}^{D} Desired indoor temperature of house h at t (°C).

$\tan(\theta_g)$ Power factor limit of DG g.

$\tan(\theta_b^{\mathrm{C}}), \tan(\theta_b^{\mathrm{D}})$ Power factor limits of ESS b.

$\tan(\theta^{\mathrm{PCC,max}})$ Power factor limits at PCC.

$\tan\left(\varphi_h^{\mathrm{H}}\right), \tan\left(\varphi_h^{\mathrm{O}}\right)$ Power factor of HVAC and non-HVAC load at house h.

$V_{\mathrm{thr}}^{\max}, V_{\mathrm{thr}}^{\min}$ Maximum/Minimum voltage thresholds beyond which voltage deviation will be minimized (p.u.).

$V^{\max}, V^{\min}$ Maximum/Minimum voltage limits (p.u.).

V_{ht}^{LS} Cost of load curtailment of house h at t (\$/kWh).

α_{ht} Percent of curtailable load of house h at period t.

δ_{ht}	Allowed indoor temperature deviation of house h during period t (°C).
$\eta_b^{\mathrm{C}}, \eta_b^{D}$	ESS b charging/discharging efficiency.
η_h	Coefficient of performance of HVAC in house h.
κ_g	Operating Cost of DG g at the point of $P_g^{\min}$ (\$/h).
$\lambda_{gt}(m)$	Marginal cost of the m-th block of energy offer by DG g during period t (\$/kWh).
λ_t^{PCC}	Purchasing price at PCC during period t (\$/kWh).
ρ	Penalty parameter of augmented Lagrangian item.
Φ_t	General irradiance of the building's surroundings during period t (kW/m^2).
ω_{ht}	Discomfort cost of house h at period t (\$/°C).
$\triangle t$	Time duration of each period (h).

1. Introduction

A microgrid can be defined as a low-voltage distribution system comprising various distributed energy resources (DERs) that are co-located with energy loads [1]. It can be grid-connected, exchanging power with the utility through the point of common coupling (PCC). If the utility system faults, a microgrid automatically transforms from grid-connected mode into islanded mode and continues to serve its islanded portion. By integrating renewable generation, energy storage devices, demand response (DR), and information and communication technology, a microgrid provides a new means of supplying electricity that is highly reliable and more cost-effective, produces fewer emissions [2], and encourages interaction with customers [3]. The benefits of microgrids have prompted a growing amount of research from both academia and industry [4].

Typically, a microgrid central controller (MCC) performs energy management for a microgrid [5]. The MCC determines the output of distributed generators (DGs), the charging/discharging power of energy storage systems (ESSs), and the exchanged power at the PCC by solving a centralized optimization problem subject to various constraints [6]. The growth of DERs, ESSs, electric vehicles, and DR is bringing unprecedented opportunities to the electricity distribution system while presenting utilities, end users, and other participants (e.g., microgrids) in distribution systems with severe challenges in complex coordination and integration. For that reason, this paper proposes a new transactive energy-based distributed energy management system for community microgrids. The proposed system is efficient and scalable while preserving customers' privacy.

1.1. Literature Review

In general, the vast majority of proposed microgrid energy management systems are based on solving a centralized optimization problem. A deterministic programming model that ignores the uncertainty of renewable generation is proposed in [7], and stochastic and robust programming models that consider the uncertainty of renewable generation are described in [8] and [9], separately. The scheduling of a multi–energy source microgrid is investigated in [10]. The thermal dynamics of buildings are included in the optimization in [11]. However, network constraints have mostly been ignored in most of the existing literature. Under network constraints, the voltage and power factor limits, as well as line thermal limits, may be violated by the solution. To address this issue, microgrid energy management that considers the distribution network is proposed in [12]. The DistFlow model of network constraints is integrated into the microgrid energy management system in [13] and the distribution management system in [14], respectively. Specifically, the nonconvex power flow constraints are relaxed into convex second-order cones [15] and then included in the optimization model as constraints. The relaxed convex DistFlow model preserves the accuracy of the power flow model while improving the solution efficiency and thus has become popular in recent years [16].

Although centralized optimization–based microgrid energy management is straightforward and easy to implement, it poses two problems. First, consumer energy consumption is mostly considered to be a fixed or interruptible load subject to direct load control. However, customers are usually very careful about allowing a utility or an MCC to directly control their appliances—such as water heaters and heating, ventilation, and air-conditioning (HVAC) systems—for various reasons, including safety and privacy protection. Second, the centralized optimization model is subject to "the curse of dimensionality": as the number of customers increases, the solution efficiency decreases rapidly. To overcome these issues, distributed optimization models based on dual decomposition are proposed, as described in [17]. The energy management problem is formulated as a convex optimization, and then a dual decomposition algorithm is used to decouple it into a subproblem of DERs and a subproblem of each customer. The information exchange between MCC and customers is limited to Lagrange multipliers and expected purchasing energy. The idea is applied to the problem of networked microgrid management in [18], Within this work, each microgrid energy management system iteratively exchanges a small amount of information with its neighboring microgrid energy management system, and locally optimizes the schedule of the corresponding microgrid. Other distributed optimization techniques, such as alternating direction method of multipliers (ADMM) [19], game approach [20], and predictor corrector proximal multiplier (PCPM) [21] have also been proposed for microgrid scheduling. Still, the network constraints are largely ignored in these papers. Distributed optimal power flow (OPF) with network constraints was proposed in [22]. The convex formulation of OPF is decomposed into several regions by ADMM to reduce the dimension of the problem and improve the solution efficiency. Another region-based distributed optimization approach to the OPF problem is proposed in [23], in which ADMM is tested in the context of nonconvex optimization. In [24], ADMM is used to solve a multi-period OPF problem with a convex power flow approximation.

It has been demonstrated that ADMM can be very efficient for solving large-scale OPF problems in a parallel environment. Nevertheless, [22], [23], and [24] are focused on the

Table 1: Comparison of models and algorithms in existing literature

Reference	Distributed Algorithm	Power Flow	Network Loss Objective	Voltage Limits	Power Factor Limits	Building Thermal Model	Nonconvex Problem
[7]							x
[8]							x
[9]							x
[10]							x
[11]						x	
[12]		x	x	x	x		x
[13]		x	x	x	x	x	x
[14]		x		x		x	x
[17]	x						
[18]	x						
[19]	x					x	x
[20]	x					x	x
[21]	x	x	x	x			
[22]	x	x					
[23]	x	x		x			x
[24]	x	x		x			
[25]	x	x	x	x			
[26]	x	x		x			
[27]	x	x		x			
[28]	x	x	x	x			
[29]	x	x		x			x
This paper	x	x	x	x	x	x	x

transmission-level OPF problem, in which DGs, ESSs, and responsive demand are neglected. For distribution systems, distributed control of reactive power based on ADMM is proposed in [25]. The network constraints are modeled using the convex DistFlow model. In [26], an online ADMM with regret is proposed for the distributed energy management of a networked microgrid system. The proposed algorithm does not require any forecast for DERs to proceed and performs better than the offline algorithm with inaccurate predictions. A distributed OPF for microgrids considering phase balance is proposed in [27]. The nonconvex problem is relaxed into a convex one by the semidefinite programming (SDP) relaxation technique. The uncertainty of renewable generation is captured by a decentralized stochastic OPF in [28]. Note that the optimization models in [25], [26], [27], and [28] are all convex, as nonconvexity might lead to nonconvergence of the distributed algorithms. To preserve the convexity, neither the startup and shutdown of DGs, nor the thermal dynamic characteristics of houses, are considered. The practical applicability of distributed optimization in the context of nonconvex formulation is evaluated in [29]. A multi-period OPF problem considering household agents with shiftable loads and nonconvex AC power flow is formulated and solved by ADMM. The results of the simulation indicate that the AC power

flow and discrete decision variables do not appear to cause convergence issues. This work brings distributed control of microgrids several steps closer to reality. Nevertheless, the startup and shutdown of DGs, charging/discharging of ESSs, power factor limits of DERs, various DRs, and building thermal dynamics are neglected. In view of the limitations of existing studies, we propose a distributed, efficient, scalable, and privacy-preserving energy management system for community microgrids that considers both the network operational constraints and building thermal dynamics. The algorithm can yield convergence without assumptions like strict convexity. The differences between the existing literature and this paper are listed in Table 1.

1.2. Contributions and Outline

In this paper, we develop a new transactive energy-based distributed energy management system for a community microgrid based on [13]. Transactive energy is a set of economic and control mechanisms that allow a dynamic balance of supply and demand across the entire electrical infrastructure using value (e.g., price) as a key operational parameter [30]. Under this framework, residential appliances are directly controlled by their owners, rather than by the MCC, to ensure autonomy and protect customer privacy. Customers exchange information with the MCC and schedule their appliances based on what is most economically beneficial rather than on control commands of the MCC. In addition, the slow thermal dynamic characteristics of buildings make them equivalent to thermal storage facilities, providing home energy management systems (HEMSs) extra flexibility in scheduling HVAC systems. On the one hand, this framework allows customers to make adjustments based on their level of comfort and the cost of electricity. On the other hand, it allows system operators to align customer behaviors with their system-level interests (e.g., voltage regulation, loss reduction, power factor correction). The unique contributions of this paper are as follows:

1. A detailed thermal dynamic model of the house is integrated into the distributed energy management system for community microgrids, which enables intelligent control of the HVAC system with autonomy and privacy for customers. The proposed distributed optimization considering thermal dynamic characteristics of houses is validated on a test system.
2. Because of the large number of binary variables (on/off for HVAC systems, startup and shutdown of DGs, and charging/discharging of ESSs), the optimization problem is nonconvex, leading to nonconvergence of traditional dual decomposition. The ADMM algorithm is introduced to decompose the nonconvex optimization into parallel subproblems of DERs and HEMSs. Results of simulations show that the ADMM algorithm can still converge without assumptions like strict convexity or finiteness.

Besides, the proposed transactive energy-based distributed energy management scheme has some important features with practical significance. First, the scheduling decisions for customer loads and DERs are private economic transactions guided by temporal price signals, which are updated iteratively. The proposed energy management optimizes the scheduling of DERs and customers in a way that respects both network operational constraints and the autonomy and privacy of customers. This has become an increasingly

important trend for reliable power system operation in light of the deregulated market structure, increasing penetration of DERs and emerging intelligent residential load management. Second, the network power flow constraints are considered in the proposed distributed energy management to ensure secure and economical operation of the community microgrid. The integration of the network constraints also makes the price signals locational, which enables the adjustment of loads and generation at specific buses.

The rest of the paper is organized as follows. Building thermal dynamics are introduced in Section II, and centralized optimization-based microgrid energy management is presented in Section III. Distributed energy management is proposed in Section IV and demonstrated on a community microgrid in Section V. Conclusions are drawn in Section VI.

2. System Model

2.1. Building Thermal Dynamic Model

A community microgrid is typically supported by numerous local generation sources and ESSs to ensure a reliable electricity supply to customers, which are normally a number of houses. In this paper, each house is assumed as a large room with uniformly distributed indoor temperature. The house envelope (i.e., walls and roof) is equivalently modeled as a thin layer inside the walls. The inner walls and indoor items are concentrated in a thin layer inside the room. Based on these assumptions, a first order linear model could be established for the thermal dynamics of a house as follows [31]:

$$C_h^{\mathrm{M}} \frac{dT_h^{\mathrm{M}}}{dt} = \frac{1}{R_h^{\mathrm{M}}} \left(T_h^{\mathrm{In}} - T_h^{\mathrm{M}}\right) + A_h p_h^s \Phi_h^s \tag{1}$$

$$C_h^{\mathrm{E}} \frac{dT_h^{\mathrm{E}}}{dt} = \frac{1}{R_h^{\mathrm{E}}} \left(T_h^{\mathrm{In}} - T_h^{\mathrm{E}}\right) + \frac{1}{R_h^{\mathrm{EA}}} \left(T^{\mathrm{A}} - T_h^{\mathrm{E}}\right) \tag{2}$$

$$\begin{aligned} C_h^{\mathrm{In}} \frac{dT_h^{\mathrm{In}}}{dt} \quad = \quad & \frac{1}{R_h^{\mathrm{A}}} \left(T^{\mathrm{A}} - T_h^{\mathrm{In}}\right) + \frac{1}{R_h^{\mathrm{M}}} \left(T_h^{\mathrm{M}} - T_h^{\mathrm{In}}\right) \\ & + \frac{1}{R_h^{\mathrm{E}}} \left(T_h^{\mathrm{E}} - T_h^{\mathrm{In}}\right) \\ & + A_h \left(1 - p_h^s\right) \Phi_h^s + \left(u_{ht}^H - u_{ht}^C\right) \eta_h P_h^H \end{aligned} \tag{3}$$

Equation (1) represents the energy balance for the thermal accumulating layer of the inner walls and floor. This layer receives energy from radiation through the windows and exchanges heat with the indoor air by convection. The building envelope exchanges heat by convection with both the inside and the outside of the building as formulated in Equation (2). Note that T^A is the ambient temperature as a combination of the outside temperature and solar irradiance on the residential building outer wall. The energy balance for indoor air is formulate as Equation (3). Note that the indoor air exchanges heat with the outside via ventilation and via conduction through the windows. C_h^{In}, C_h^{M}, C_h^{E}, R_h^{A}, R_h^{M}, R_h^{E}, R_h^{EA}, and p_h^s are the thermal parameters of house h. Estimation of the building thermal parameters based on historical measurements is another important research topic with extensively

referenced literature. Commonly used methods include Maximum Likelihood (ML) estimation [32] and finite difference approximation [33]. To be succinct, equation (1) - (3) could be rewritten as the linear state-space model (4) in continuous time.

$$\frac{d\boldsymbol{T}_h}{dt} = \boldsymbol{A}_h \boldsymbol{T}_h + \boldsymbol{B}_h \boldsymbol{U}_h \tag{4}$$

where $\boldsymbol{T}_h = \left[T_h^{\mathrm{In}}, T_h^M, T_h^E\right]$ is the state vector, which indicates the temperatures at different layers of the house. $\boldsymbol{U}_h = \left[T^A, \Phi, \left(u_h^H - u_h^C\right)\eta_h P_h^H\right]$ is the input vector, which includes the ambient temperature, solar irradiance and heat transferred by the HVAC system. The coefficients of matrices $\boldsymbol{A}_h$ and $\boldsymbol{B}_h$ of a house h could be calculated based on its thermal parameters. By Euler discretization, we could transform the state-space model in continuous time (4) into an equivalent discrete time model (5).

$$\boldsymbol{T}_{h,t+1} = \boldsymbol{A}_h^{disc} \boldsymbol{T}_{h,t} + \boldsymbol{B}_h^{disc} \boldsymbol{U}_{h,t} \quad \forall h, \forall t \tag{5}$$

The matrices $\boldsymbol{A}_h^{disc}$ and $\boldsymbol{B}_h^{disc}$ are constant and could be calculated based on $\boldsymbol{A}_h$, $\boldsymbol{B}_h$ and the time step size. We will use this discrete time model in the following problem formulation. More details on the modeling and parameter estimation of the house can be found in [31]. The indoor temperature for house h is limited in an allowable range as in (6).

$$T_{ht}^D - \delta_{ht} \leq T_{ht}^{\mathrm{In}} \leq T_{ht}^D + \delta_{ht} \tag{6}$$

2.2. HVAC System

An HVAC system is usually controlled by a thermostat with a relay circuit. The HVAC is switched on when the indoor temperature reaches the upper limit, then continues running until the lower limit is reached. Thermostats based on this automatic temperature control scheme are widely used. Owing to the thermal inertia of a house, the indoor temperature changes gradually. A house could be considered a thermal storage facility that provides the HEMS with extra flexibility in scheduling the HVAC system. Specifically, the HVAC system can be switched on to precool/preheat the house during times when electricity prices are low or renewable generation is high. Thus, the house can ride through peak-price periods without high electricity consumption and still maintain the indoor temperature within an allowable range. This method is expected to achieve significant electricity cost savings compared with autonomous temperature control.

3. Centralized Microgrid Energy Management

3.1. Objective

In this section, a centralized optimization problem for the energy management of community microgrids is formulated. The objective is to minimize a virtual cost associated with different system performance indices, as in (7). Specifically, the piecewise linear operation cost and startup costs of DGs are represented in line 1. Note that the startup cost U_{gt} is a function of u_{gt} and $u_{g,t-1}$. Resident discomfort due to indoor temperature deviations and voluntary load shedding is in line 2; the energy purchasing/selling cost/benefit at the PCC and the degradation costs of ESSs are in line 3; total voltage deviation is described in lines 4 and 5; and the network power loss and the total absolute value of the reactive

power exchange at the PCC, which indicates the power factor at the PCC, are included in line 6. All objectives are summed into a single objective function with corresponding weightings. The weighting coefficients W_C, W_V, W_L, and W_Q can be determined by the analytical hierarchy process (AHP) [34], which is an effective tool for dealing with complex decision making and helping the decision maker to set priorities and make the best decision. With AHP, the system operators can calculate the weighting coefficients of all objectives based on the pairwise comparison of the relative importance of any two objectives. More details on how to calculate the weighting coefficients by AHP are introduced in Section V.

$$
\begin{aligned}
\min \quad & W_C \left\{ \sum_{t=1}^{N_T} \sum_{g=1}^{N_G} \left[\sum_{m=1}^{N_I} \lambda_{gt}(m) p_{gt}(m) \triangle t + \kappa_i u_{gt} \triangle t + U_{gt} \right] \right. \\
& + \sum_{t=1}^{N_T} \sum_{h=1}^{N_H} \left(\omega_{ht} \left| T_{ht}^{\mathrm{In}} - T_{ht}^{D} \right| \triangle t + V_{ht}^{LS} P_{ht}^{LS} \triangle t \right) \\
& \left. + \sum_{t=1}^{N_T} \lambda_t^{\mathrm{PCC}} P_t^{\mathrm{PCC}} \triangle t + \sum_{t=1}^{N_T} \sum_{b=1}^{N_B} C_{bt} \left(P_{bt}^{\mathrm{C}} + P_{bt}^{\mathrm{D}} \right) \triangle t \right\} \\
& + W_V \left[\sum_{t=1}^{N_T} \sum_{n=1}^{N_N} V_{nt}^2 - \left(V_{\mathrm{thr}}^{\max} \right)^2 : \left(V_{nt} > V_{\mathrm{thr}}^{\max} \right) \right. \\
& \left. + \sum_{t=1}^{N_T} \sum_{n=1}^{N_N} \left(V_{\mathrm{thr}}^{\min} \right)^2 - V_{nt}^2 : \left(V_{nt} < V_{\mathrm{thr}}^{\min} \right) \right] \triangle t \\
& + W_L \left(\sum_{t=1}^{N_T} \sum_{j=1}^{N_F} r_f l_{ft} \right) \triangle t + W_Q \left(\sum_{t=1}^{N_T} \left| Q_t^{\mathrm{PCC}} \right| \right) \triangle t
\end{aligned} \tag{7}
$$

For the customer discomfort cost due to indoor temperature deviations in line 2, it is assumed that each household will set its desired indoor temperature T_{ht}^{D} and a maximum allowed indoor temperature deviation δ_{ht} for each time period in the HEMS. Then, the HEMS will control the HVAC system so that the indoor temperature lies within the acceptable range $[T_{ht}^{D} - \delta_{ht},\, T_{ht}^{D} + \delta_{ht}]$. Within this acceptable range, the closer the current indoor temperature T_{ht}^{In} is to the desired temperature T_{ht}^{D}, the more comfortable the customer will be. Therefore, to drive the indoor temperate as close to the desired temperature as possible, we define the customer discomfort cost for the time period t as $\omega_{ht} \left| T_{ht}^{\mathrm{In}} - T_{ht}^{D} \right|$, where ω_{ht} can be viewed as the price (\$/°C) that household h is paid if the indoor temperature T_{ht}^{In} deviates by 1°C from the desired temperature T_{ht}^{D} in the current time period. The values of ω_{ht} are directly set by customers through the HEMS in each house.

3.2. Constraints

3.2.1. DG Constraints

In this paper, the convex quadratic cost function of DGs is approximated by piecewise linearization. First, the controllable range of the power output of DG g, $[P_g^{\min},\, P_g^{\max}]$ is divided into N_I energy blocks $\{p_{gt}(1),\, p_{gt}(2),\, \ldots\, ,p_{gt}(N_I)\}$. For each energy block, the

quadratic cost curve is estimated by a linear segment. Then, the operating cost DG g could be approximated as equation (8). Due to the convexity of the approximation of the cost function, it is guaranteed that all DGs will be dispatched in such a way that an energy block with a larger marginal cost will not be loaded unless the ones with lower marginal cost are fully loaded. The generation limits for each energy block of the piecewise approximation are enforced by (9). The power of DG g during time period t is represented as (10). The minimum and maximum power of DGs are enforced by (11). The power factor and capacity limits of DGs are ensured by (12) and (13).

$$OC_{gt}\left(P_{gt},\, u_{gt}\right) = \sum_{m=1}^{N_I} \lambda_{gt}(m) p_{gt}(m) \triangle t + \kappa_g u_{gt} \triangle t \quad \forall g,\, \forall t \tag{8}$$

$$0 \leq p_{gt}(m) \leq p_{gt}^{\max}(m) \quad \forall g,\, \forall t,\, \forall m \tag{9}$$

$$P_{gt} = \sum_{m=1}^{N_I} p_{gt}(m) + u_{gt} P_g^{\min} \quad \forall g,\, \forall t \tag{10}$$

$$u_{gt} P_g^{\min} \leq P_{gt} \leq u_{gt} P_g^{\max} \quad \forall g,\, \forall t \tag{11}$$

$$-\tan(\theta_g) P_{gt} \leq Q_{gt} \leq \tan(\theta_g) P_{gt} \quad \forall g,\, \forall t \tag{12}$$

$$(P_{gt})^2 + (Q_{gt})^2 \leq S_g^2 \quad \forall g,\, \forall t \tag{13}$$

3.2.2. ESS Constraints

ESS charging and discharging power is constrained by (14) and (15). The charging and discharging states of an ESS are mutually exclusive, enforced by (16). The state of charge (SOC) of an ESS at the end of the current time period t is determined by the SOC in the previous time period $t-1$, plus/minus the energy charged/discharged during the current time period as in (17). The SOC of an ESS is limited by (18). The power loss during the charging and discharging process is described with parameter η_b^{C} and η_b^{D}. The power factor of the inverter associated with an ESS in charging and discharging states is limited by (19) and (20). The capacity limit of the ESS inverter is ensured by (21) and (22).

$$0 \leq P_{bt}^{\mathrm{C}} \leq P_b^{\mathrm{C,max}} u_{bt}^{\mathrm{C}} \quad \forall b,\, \forall t \tag{14}$$

$$0 \leq P_{bt}^{\mathrm{D}} \leq P_b^{\mathrm{D,max}} u_{bt}^{\mathrm{D}} \quad \forall b,\, \forall t \tag{15}$$

$$u_{bt}^{\mathrm{C}} + u_{bt}^{\mathrm{D}} \leq 1 \quad \forall b,\, \forall t \tag{16}$$

$$SOC_{bt} = SOC_{b,t-1} + P_{bt}^{\mathrm{C}} \eta_b^{\mathrm{C}} \triangle t - P_{bt}^{\mathrm{D}} \frac{1}{\eta_b^{\mathrm{D}}} \triangle t \quad \forall b,\, \forall t \tag{17}$$

$$SOC_{bt}^{\min} \leq SOC_{bt} \leq SOC_{bt}^{\max} \quad \forall b,\, \forall t \tag{18}$$

$$-\tan(\theta_b^{\mathrm{C}}) P_{bt}^{\mathrm{C}} \leq Q_{bt} \leq \tan(\theta_b^{\mathrm{C}}) P_{bt}^{\mathrm{C}} :\, \left(P_{bt}^{\mathrm{C}} > 0\right) \forall b,\, \forall t \tag{19}$$

$$-\tan(\theta_b^{\mathrm{D}}) P_{bt}^{\mathrm{D}} \leq Q_{bt} \leq \tan(\theta_b^{\mathrm{D}}) P_{bt}^{\mathrm{D}} :\, \left(P_{bt}^{\mathrm{D}} > 0\right) \forall b,\, \forall t \tag{20}$$

$$P_{bt} = P_{bt}^{\mathrm{D}} - P_{bt}^{\mathrm{C}} \quad \forall b,\, \forall t \tag{21}$$

$$(P_{bt})^2 + (Q_{bt})^2 \leq S_b^2 \quad \forall b,\, \forall t \tag{22}$$

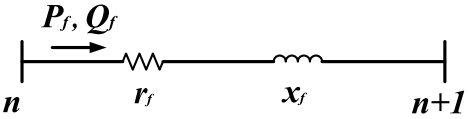

Figure 1: Example of a distribution feeder

3.2.3. Load Constraints

For each house, the total load equals the HVAC load plus the aggregated non-HVAC loads as in equation (23) and (24). The heating and cooling states of a HVAC system are mutually exclusive, as is guaranteed by constraint (25). The voluntary load shedding of house h during time period t is limited by a certain percentage of the aggregated load specified by the customer, as shown in constraint (26). The reactive power is curtailed along with real power based on an assumed power factor for each house as in (27). Note that the thermal dynamic characteristics of a house (5) and the indoor temperature requirements (6) should be included as load constraints as well.

$$P_{ht} = \left(u_{ht}^{\mathrm{H}} + u_{ht}^{\mathrm{C}}\right) P_h^{\mathrm{H}} + P_{ht}^{\mathrm{O}} \quad \forall h, \forall t \tag{23}$$

$$Q_{ht} = tan\left(\varphi_h^{\mathrm{H}}\right)\left(u_{ht}^{\mathrm{H}} + u_{ht}^{\mathrm{C}}\right) P_h^{\mathrm{H}} + Q_{ht}^{\mathrm{O}} \quad \forall h, \forall t \tag{24}$$

$$u_{ht}^{\mathrm{H}} + u_{ht}^{\mathrm{C}} \leq 1 \quad \forall h, \forall t \tag{25}$$

$$0 \leq P_{ht}^{\mathrm{LS}} \leq \alpha_{ht} P_{ht}^{\mathrm{O}} \quad \forall h, \forall t \tag{26}$$

$$Q_{ht}^{\mathrm{LS}} = tan\left(\varphi_h^{O}\right) P_{ht}^{\mathrm{LS}} \quad \forall h, \forall t \tag{27}$$

3.2.4. Network Constraints

Given a distribution feeder as in Fig. 1, bus n is the sending end and bus $n+1$ is the receiving end. The steady-state power flow can be modeled by the DistFlow equations (28) - (31) [16]. The voltage drop along the feeder is described as in (28). Both real and reactive power should be balanced for each bus, which is enforced by (29) and (30) separately. $\mathbf{M_f}$ and $\mathbf{M_l}$ are the incidence matrices of the feeder flow and feeder loss for the sending end bus n. $\mathbf{M_f}\,(n,\, f)$ is 1 if bus n is the sending end of feeder f, -1 if bus n is the receiving end of feeder f , and zero if neither terminal of feeder f is connected to bus n. $\mathbf{M_l}\,(n,\, f)$ is 1 if bus n is the receiving end of feeder f and zero for all other elements. Particularly for the PCC bus, P_t^{PCC} and Q_t^{PCC} should be added to (29) and (30), separately. For the accuracy of the conic relaxation in DistFlow, the exactness of the convex relaxation is probed in [35], and the results of conic relaxation–based optimal power flow (OPF) are compared with those for the standard nonlinear programming–based OPF for various IEEE test systems in [36]. Equation (32) represents the voltage limits of buses and (33) the line flow limits of feeders. Note that by directly taking the square of nodal voltage V_{nt}^2 as a variable, equations (28) and (32) are linear, and equation (31) is a second order cone.

$$V_{n+1,t}^2 = V_{nt}^2 - 2\left(r_f P_{ft} + x_f Q_{ft}\right) + \left(r_f^2 + x_f^2\right) l_{ft} \tag{28}$$

$$\sum_{g\in\mathcal{G}_n} P_{gt} + \sum_{b\in\mathcal{B}_n} P_{bt} - \sum_{h\in\mathcal{H}_n} \left(P_{ht} - P_{ht}^{\mathrm{LS}}\right) + \sum_{v\in\mathcal{V}_n} P_{vt} = \sum_{f\in\Omega} \mathbf{M_f} P_{ft} + \sum_{f\in\Omega} \mathbf{M_l} r_f l_{ft} \tag{29}$$

$$\sum_{g\in\mathcal{G}_n} Q_{gt} + \sum_{b\in\mathcal{B}_n} Q_{bt} - \sum_{h\in\mathcal{H}_n} \left(Q_{ht} - Q_{ht}^{\mathrm{LS}}\right) + \sum_{v\in\mathcal{V}_n} Q_{vt} = \sum_{f\in\Omega} \mathbf{M_f} Q_{ft} + \sum_{f\in\Omega} \mathbf{M_l} x_f l_{ft} \tag{30}$$

$$(P_{ft})^2 + (Q_{ft})^2 \leq V_{nt}^2 l_{ft} \quad \forall\, f, \forall\, t \tag{31}$$

$$\left(V^{\min}\right)^2 \leq V_{nt}^2 \leq (V^{\max})^2 \quad \forall\, n, \forall\, t \tag{32}$$

$$l_{ft} \leq \left(I_f^{\max}\right)^2 \quad \forall f, \forall t \tag{33}$$

3.2.5. PCC Constraints

The maximum power at the PCC is limited by the line capacity or previously established contracts, as in (34). Similarly, the power factor of the community microgrid seen by the utility at the PCC is limited as in (35). In addition, the voltage at the PCC is assumed at fixed values, which depend on the operating condition of the utility system. This assumption is presented in equation (36).

$$-P^{\mathrm{PCC,max}} \leq P_t^{\mathrm{PCC}} \leq P^{\mathrm{PCC,max}} \quad \forall\, t \tag{34}$$

$$-\tan(\theta^{\mathrm{PCC,max}}) \left|P_t^{\mathrm{PCC}}\right| \leq Q_t^{\mathrm{PCC}} \leq \tan(\theta^{\mathrm{PCC,max}}) \left|P_t^{\mathrm{PCC}}\right| \tag{35}$$

$$V_t^{\mathrm{PCC}} = V^{\mathrm{Fix}} \tag{36}$$

Centralized community microgrid energy management can be reformulated as a mixed-integer conic programming (MICP) by recasting all logic items in the objective function and constraints into linear or mixed-integer linear (MIL) form. Specifically, by introducing a binary variable, the startup cost of DGs (in line 1) could be represented in MIL form [37]. The MIL reformulation of the logic expression of voltage deviations in (7) and absolute functions in (7) and (35) can be found in [13]. The logical terms in the ESS inverters' power factor constraint (19) and (20) can be reformulated into MIL form, as (37) and (38) by the reuse of binary charging/discharging indicators. In general, this centralized optimization problem could be solved by various commercial MICP solvers.

$$-S_b u_{bt}^{\mathrm{D}} - \tan(\theta_b^{\mathrm{C}}) P_{bt}^{\mathrm{C}} \leq Q_{bt} \leq \tan(\theta_b^{\mathrm{C}}) P_{bt}^{\mathrm{C}} + S_b u_{bt}^{\mathrm{D}} \forall b, \forall t \tag{37}$$

$$-S_b u_{bt}^{\mathrm{C}} - \tan(\theta_b^{\mathrm{D}}) P_{bt}^{\mathrm{D}} \leq Q_{bt} \leq \tan(\theta_b^{\mathrm{D}}) P_{bt}^{\mathrm{D}} + S_b u_{bt}^{\mathrm{C}} \forall b, \forall t \tag{38}$$

4. Transactive Energy-based Distributed Microgrid Energy Management

The centralized optimization model is straightforward and easy to solve. However, to solve the optimization, MCC requires access to the information on user settings, house thermal parameters, and other load information for all houses, whereas customers generally prefer to withhold detailed information on energy consumption behind the meter and to control their home appliances themselves. In addition, the dimension of the optimization

increases significantly as the number of houses increases. Therefore, a distributed, scalable, privacy-preserving microgrid energy management system is proposed in this section.

The centralized optimization model has a separable structure, since only constraints (29) and (30) are complicating constraints involving variables from both the microgrid and the house levels. For a convex optimization problem, dual decomposition can converge to a global optimal solution. However, when the problem is not convex, such as (7), even finding a feasible solution becomes difficult. For this reason, the ADMM is introduced to facilitate convergence without assumptions like strict convexity or finiteness. First, the complicating constraints (29) and (30) are integrated into the objective function as Lagrangian items. The corresponding Lagrangian multipliers are the shadow prices for real and reactive power, separately. Then, the centralized Lagrangian optimization model is easily decomposed into optimization subproblems at the microgrid and house levels, which are solved by the MCC and the HEMSs separately. The solutions are coordinated by an iterative process [38].

The term "transactive" comes from considering that the scheduling decisions for MCC and HEMSs may be analogous to or may literally be economic transactions. Specifically, the DERs and HEMSs receive locational and temporal energy prices, then decide the amount of generation or consumption considering their private interests. The introduction of transactive energy benefits both customers and utilities. It helps customers to shave their electricity bills by shifting or curtailing their usage, or deploying ESSs and DGs. And it allows utilities to leverage demand-side flexibilities and resources to meet grid needs (such as voltage regulation and loss minimization) instead of building traditional infrastructure.

$$\begin{aligned} R_{nt}^{(k)} \quad = \quad & \sum_{g\in\mathcal{G}_n} P_{gt}^{(k)} + \sum_{b\in\mathcal{B}_n} P_{bt}^{(k)} + \sum_{v\in\mathcal{V}_n} P_{vt} - \sum_{f\in\Omega} \mathbf{M_f} P_{ft}^{(k)} \\ & - \sum_{f\in\Omega} \mathbf{M_l} r_f l_{ft}^{(k)} - \sum_{h\in\mathcal{H}_n} \left(P_{ht}^{(k)} - P_{ht}^{\mathrm{LS,(k)}} \right) \end{aligned} \tag{39}$$

Initially set $k \leftarrow 0$, and the HEMSs schedule their appliances randomly and communicate them to the MCC. In the meantime, the MCC sets initial price curves for each bus and schedules the microgrid level resources randomly. At the beginning of each iteration, the MCC updates the unbalanced power at each bus according to equation (39) and communicates the prime residual $R_{nt}^{(k)}$ and price signal $\lambda_{nt}^{(k)}$ to corresponding HEMSs connected to each bus. Then the following happens.

1. The HEMS of each house solves the HEMS subproblem as follows:

$$\begin{aligned} \min \qquad & W_C \left\{ \sum_{t=1}^{N_T} \left(\omega_{ht} \left| T_{ht}^{\mathrm{In}} - T_{ht}^{D} \right| + V_{ht}^{LS} P_{ht}^{LS} \right) \triangle t \right\} \\ & - \sum_{t=1}^{N_T} \lambda_{nt}^{(k)} \left[R_{nt}^{(k)} + \left(P_{ht}^{(k)} - P_{ht}^{\mathrm{LS,(k)}} \right) - \left(P_{ht} - P_{ht}^{\mathrm{LS}} \right) \right] \\ & + \frac{\rho}{2} \left\| \mathbf{R}_n^{(k)} + \left(\mathbf{P}_h^{(k)} - \mathbf{P}_h^{\mathrm{LS,(k)}} \right) - \left(\mathbf{P}_h - \mathbf{P}_h^{\mathrm{LS}} \right) \right\|_2^2 \end{aligned} \tag{40}$$

s.t.

$$(5),\ (6) \text{ and } (22)-(26)$$

2. The MCC solves the MCC subproblem as follows:

$$
\begin{aligned}
\min \quad & W_C \left\{ \sum_{t=1}^{N_T} \sum_{g=1}^{N_G} \left[\sum_{m=1}^{N_I} \lambda_{gt}(m) p_{gt}(m) \triangle t + \kappa_g u_{gt} \triangle t + U_{gt} \right] \right. \\
& \left. + \sum_{t=1}^{N_T} \lambda_t^{\mathrm{PCC}} P_t^{\mathrm{PCC}} \triangle t + \sum_{t=1}^{N_T} \sum_{b=1}^{N_B} C_{bt} \left(P_{bt}^{\mathrm{C}} + P_{bt}^{\mathrm{D}} \right) \triangle t \right\} \\
& + W_V \left[\sum_{t=1}^{N_T} \sum_{n=1}^{N_N} V_{nt}^2 - \left(V_{\mathrm{thr}}^{\max} \right)^2 : \left(V_{nt} > V_{\mathrm{thr}}^{\max} \right) \right. \\
& \left. + \sum_{t=1}^{N_T} \sum_{n=1}^{N_N} \left(V_{\mathrm{thr}}^{\min} \right)^2 - V_{nt}^2 : \left(V_{nt} < V_{\mathrm{thr}}^{\min} \right) \right] \triangle t \\
& + W_L \left(\sum_{t=1}^{N_T} \sum_{j=1}^{N_F} r_f l_{ft} \right) \triangle t + W_Q \left(\sum_{t=1}^{N_T} \left| Q_t^{\mathrm{PCC}} \right| \right) \triangle t \\
& - \sum_{t=1}^{N_T} \sum_{n=1}^{N_N} \lambda_{nt}^{(k)} \left[R_{nt}^{(k)} - \sum_{g \in \mathcal{G}_n \bigcup \mathcal{B}_n} P_{gt}^{(k)} + \sum_{g \in \mathcal{G}_n \bigcup \mathcal{B}_n} P_{gt} \right] \\
& + \frac{\rho}{2} \sum_{n=1}^{N_N} \left\| \mathbf{R}_n^{(k)} - \sum_{g \in \mathcal{G}_n \bigcup \mathcal{B}_n} \mathbf{P}_g^{(k)} + \sum_{g \in \mathcal{G}_n \bigcup \mathcal{B}_n} \mathbf{P}_g \right\|_2^2
\end{aligned} \tag{41}
$$

s.t.

$$
(8) - (21) \text{, and } (27) - (35)
$$

At the end of each iteration, the HEMSs communicate their updated schedules $P_{ht}^{(k)}$, $Q_{ht}^{(k)}$ and $P_{ht}^{\mathrm{LS,(k)}}$, $Q_{ht}^{\mathrm{LS,(k)}}$ to the MCC. Then the MCC updates the prime residual $R_{nt}^{(k+1)}$, dual residual $S_{nt}^{(k+1)}$ and price signal $\lambda_{nt}^{(k+1)}$ according to (39), (42) and (43), respectively. This iterative process is repeated until convergence.

$$
S_{nt}^{(k+1)} = \sum_{h \in \mathcal{H}_n} \left[\left(P_{ht}^{(k+1)} - P_{ht}^{\mathrm{LS,(k+1)}} \right) - \left(P_{ht}^{(k)} - P_{ht}^{\mathrm{LS,(k)}} \right) \right] \tag{42}
$$

$$
\lambda_{nt}^{(k+1)} = \lambda_{nt}^{(k)} - \rho R_{nt}^{(k+1)} \tag{43}
$$

A complete description of the proposed ADMM-based distributed energy management approach can be found in Algorithm 1. Compared with traditional dual decomposition, the ADMM algorithm adds an augmented Lagrangian term with a penalty factor $\rho > 0$. This augmented Lagrangian term is introduced in part to bring robustness to the dual decomposition algorithm and, in particular, to yield convergence without assumptions like strict convexity or finiteness of (7). In other words, ADMM improves the classic dual

Algorithm 1 Proposed ADMM-based Distributed Energy Management

1: **initialization** $k \leftarrow 0$. The HEMSs set their initial schedules, and send them to the MCC. The MCC sets the initial price, and schedules the microgrid level resources.
2: **repeat**
3: The MCC updates $R_{nt}^{(k)}$ for each bus, and sends $R_{nt}^{(k)}$ and $\lambda_{nt}^{(k)}$ to the HEMSs connected to that bus.
4: The HEMS of each house updates its schedule by solving the HEMS subproblem.
5: The MCC updates the schedule of microgrid level resources by solving the MCC subproblem.
6: The HEMSs send the updated total consumption and load shedding back to MCC, then the MCC updates the primal residual $R_{nt}^{(k+1)}$, dual residual $S_{nt}^{(k+1)}$ and price signal $\lambda_{nt}^{(k+1)}$ according to (39), (42) and (43), respectively;
7: $k \leftarrow k+1$;
8: **until** $\left(R_{nt}^{(k+1)} \leq R^{\max}\right) \& \left(S_{nt}^{(k+1)} \leq S^{\max}\right)$

decomposition algorithm with the superior convergence properties of augmented Lagrangian methods. Although ADMM has been applied in a variety of fields, including networked optimization, estimation, compressed sensing, and multi-agent systems, there is a lack of theoretical support for how to set the algorithm parameters, and its step-size ρ is typically tuned experimentally. Generally, large values of ρ place a large penalty on violations of primal feasibility and so tend to produce small primal residuals, leading to local optimum. Conversely, small values of ρ tend to reduce the dual residual, but they do so at the expense of reducing the penalty for primal feasibility, which may cause convergence issues. A reasonable stopping criterion is that both the primal and dual residuals have to be small [38]. Optimal step-size selection for constrained quadratic programming is proposed in [39]. For nonconvex consensus and sharing problems, it has been concluded that the classical ADMM converges to the set of stationary solutions, provided that the step-size ρ is chosen to be sufficiently large [40]. Nevertheless, there are still no theoretical guarantees for ADMM convergence in the nonconvex regime.

Another issue with ADMM is that a global optimum cannot be guaranteed for nonconvex optimization problems, especially when the nonconvexities are due to binary variables. Although the values of objectives could be improved by tuning parameter settings (e.g., optimality gap of subproblems, stopping criteria, and step-size), there is still no guarantee that the global optimum could be found. Nevertheless, it is often the case that ADMM converges to modest accuracy within a few tens of iterations [38].

In this proposed transactive energy-based distributed energy management approach, the MCC broadcasts the power imbalance and price signals of each bus to the corresponding HEMSs through the advanced metering infrastructures. For each house, the HEMS subproblem (40) is solved, then the total consumption $P_{ht}^{(k)}$, $Q_{ht}^{(k)}$ and voluntary load shedding $P_{ht}^{\mathrm{LS,(k)}}$, $Q_{ht}^{\mathrm{LS,(k)}}$ are communicated to the MCC. In this way, customers have absolute control over their HVAC systems and other appliances behind the meter. Also, the schedules of individual appliances and customer preferences are concealed from the MCC. Therefore, customer privacy is preserved. The exchange of information between MCC and HEMSs is

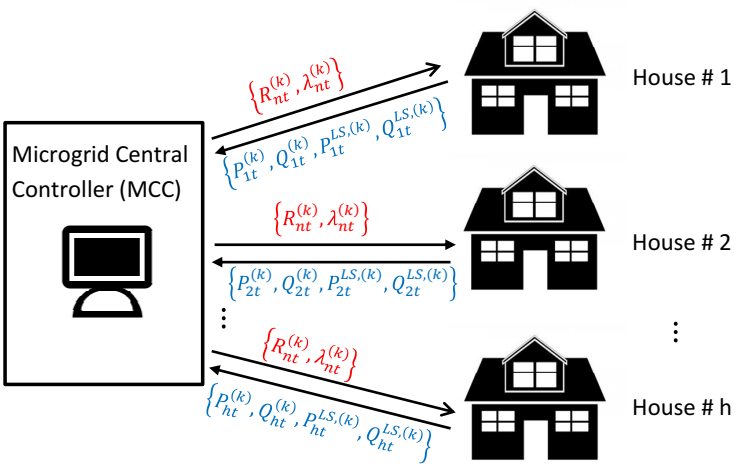

Figure 2: Exchange of Information between MCC and HEMSs

shown in Fig. 2.

The centralized energy management is MICP. In CPLEX, it is solved using the branch and cut (B&C) method, which has an exponential complexity of $O\left(2^{N_G \times N_T + N_B \times N_T + N_H \times N_T}\right)$. For the proposed distributed energy management scheme, the computational complexity of the HEMS subproblem is $O\left(2^{N_T}\right)$, while the computational complexity of the MCC subproblem is $O\left(2^{N_G \times N_T + N_B \times N_T}\right)$. Considering that the HEMS subproblems are solved in parallel, the computational complexity of the proposed distributed energy management is $\left[O\left(2^{N_G \times N_T + N_B \times N_T}\right) + O\left(2^{N_T}\right)\right] \times N_K$, where N_K is the total number of iterations. For community microgrids with multiple generators, multiple houses and multiple periods, the computational complexity of the proposed distributed energy management approach is reduced significantly.

It should be noted that only real power is transactive in the proposed model, since the reactive power load and reactive power load curtailment of a house could be determined by its real power load and real power load curtailment based on an assumed power factor. Nevertheless, the proposed model can easily be extended to make the reactive power transactive if the customers have reactive power regulation equipment installed (e.g., capacitors, PV/battery inverters with reactive power regulation).

5. Case Studies

The proposed distributed energy management was tested on a modified Oak Ridge National Laboratory microgrid test system, as shown in Fig. 3. The controller-hardware-in-the-loop (C-HIL) test system is composed of a real-time digital simulator (RTDS) for modeling the microgrid, multiple NI Compact RIOs for device-level control, a microgrid central controller (MCC), and a HEMS for each house [41]. The parameters for the DGs, PV, and ESS can be found in [13]. The system has 20 houses with a 5 kW HVAC installed in each house. The coefficients of performance (COPs) of all HVAC systems are set at $\eta_h = 3$. The desired indoor temperature is set at 23 °C with ±2°C allowed deviations. Customer discomfort cost is set at 0.05 $/°C [11]. The cost of load shedding is set at 2.0

$/kWh, and the maximum load shedding is limited to 10% of the non-HVAC load. The thermal parameters of the houses are taken from [34] (Table 7.1 in [34]). The ambient temperature and solar irradiance are the measured data of the Oak Ridge, Tennessee, area on 1 August, 2015 [42], which is a typical summer day in the southern United States.

The analysis was conducted for a 24-hour scheduling horizon with 15-min time resolution (i.e., 96 time periods in total). The forecast non-HVAC demand in house #1 and the day-ahead market prices at the PCC are shown in Fig. 4. For simplicity, all houses were assumed to have the same non-HVAC loads. The power factor of both HVAC and non-HVAC loads was assumed to be 0.9 and the power factor at the PCC is required to be no less than 0.95. The voltage at the PCC was set at 1.01 p.u., and the initial price was set as 0.1 $/kWh for all time intervals. The penalty parameter ρ is set as 0.1. All subproblems are solved using the commercial MICP solver CPLEX 12.6 on a 2.66 GHz Windows-based PC with 4 GB of RAM.

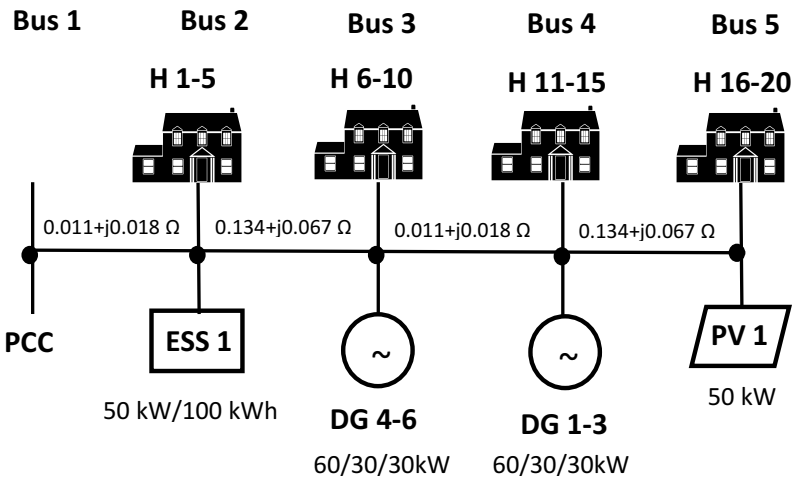

Figure 3: Community microgrid test system

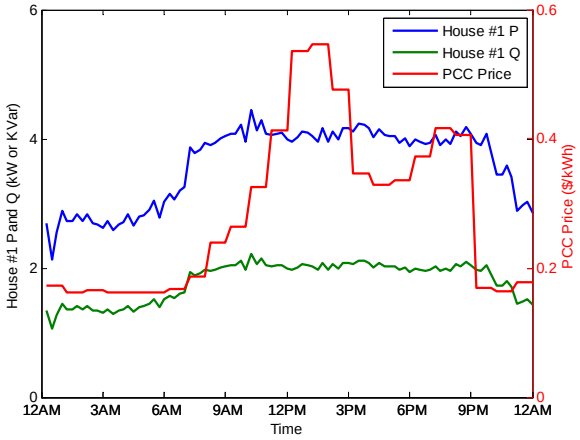

Figure 4: Non-HVAC demand in house and electricity price at the PCC

Table 2: A typical pairwise comparison matrix terms

	Operating Cost	Total Reactive Power	Voltage Deviation	Network Loss
Operating Cost	1	2	1/3	3
Total Reactive Power	1/2	1	1/5	2
Voltage Deviation	3	5	1	10
Network Loss	1/3	1/2	1/10	1

5.1. Calculating Weighting Coefficients

The calculation of the weighting coefficients for multiple objectives by the AHP is introduced in this subsection. For simplicity, the fuel and startup costs of DGs, energy purchase cost, battery degradation cost, customer discomfort, and load shedding cost are aggregated together as operating costs with weighting coefficient W_C. The process is divided into two steps. First, a pairwise comparison matrix is established by pairwise comparison of the relative importance or priority between each two objectives. For each element in the matrix, the importance of the objective at the left is compared with the importance of the objective at the top, and the ratio is entered. Second, the weighting coefficients of all objectives are retrieved by solving an eigenvalue problem. If the pairwise comparison matrix is consistent, it is rank one, and thus all its eigenvalues but one are equal to zero. This largest eigenvalue, i.e., principal eigenvalue, is unique and equals the dimension of the comparison matrix. The corresponding eigenvector, i.e., the principal eigenvector, is positive and unique. The weighting coefficients of objectives can be obtained by normalizing this principal eigenvector. In most cases, the pairwise comparison matrix is very likely to be inconsistent, especially when the number of objectives is large. According to [34], a consistency of about 10% is generally acceptable. In an inconsistent case, the principal eigenvalue is still unique and is approximately equal to the dimension of the comparison matrix. The weighting coefficients can be obtained in the same way.

A typical pairwise comparison matrix is shown in Table 2; the corresponding weighting coefficients are calculated as W_C=0.2084, W_Q=0.1171, W_V=0.6116, and W_L=0.0629. Note that the weighting coefficients are calculated based on the pairwise comparison matrix, which is established by system operators based on their own preference.

5.2. Comparing Costs of Different Cases

The total and individual objectives calculated by autonomous temperature control, centralized optimization, and the proposed distributed optimization in both grid-connected and islanded modes are compared in Table 3. In the case of autonomous control, equation (5) is solved first, then the thermostats determine the on/off status of the HVAC systems according to the internal temperature relay circuit. Given predetermined HVAC status, we solved centralized optimization and obtained the corresponding objectives as in equation (7). For easily comparing the total objective as well as individual objectives, the weighting coefficients were set as $W_C = W_Q = W_V = W_L = 1$ for all cases. Note that the weighting coefficients can be changed according to the system operator's preference [13].

Comparing the results of centralized optimization with those of autonomous control, the operating cost was reduced by 15.84% and 13.04% in grid-connected and islanded

Table 3: Costs of the community microgrid in different cases

Cases		Total Obj.	Operating Cost ($)	Loss (kWh)	Voltage Deviation (p.u.)	Reactive Power (kVarh)	Solution Time (Minutes)
Grid-Connected	Autonomous Control	659.11	636.14	21.12	1.81	0.03	<1
	Centralized Opt.	558.75	535.40	20.83	2.44	0.07	2
	Distributed Opt.	583.12	562.15	19.19	1.77	0.01	3
Islanded	Autonomous Control	718.44	691.90	22.88	3.59	0.06	<1
	Centralized Opt.	623.74	601.65	19.01	3.02	0.06	9
	Distributed Opt.	647.05	625.56	18.80	2.67	0.02	4

mode, respectively; and the system performance indices—i.e., power loss, voltage deviation and reactive power at the PCC—were almost the same. By integrating the building thermal dynamics into the optimization, the system operating cost was reduced significantly. Comparing the results of distributed optimization with those of autonomous control, the operating cost was reduced by 11.63% and 9.59% in grid-connected and islanded mode, respectively. Compared with centralized optimization, the proposed distributed optimization preserves privacy with comparable optimality.

Note that both the solution time and objective value of centralized optimization are affected by the setting of the MIP gap in CPLEX. With different MIP gap settings, the total objective value and solution time of centralized optimization in both grid-connected and islanded mode are shown in Fig. 5. Generally, the objective value is reduced as the solution time increases in a very nonlinear pattern. For a fair comparison between centralized optimization and distributed optimization, the timing of centralized optimization should be terminated when it reaches a solution as good as the distributed optimization. Based on this rule, the solution times of both methods are compared in Table 3. As can be seen, the solution efficiency of both methods is similar in grid-connected mode, but distributed optimization performs better than centralized optimization in islanded mode.

5.3. Operation in Grid-Connected Mode

The scheduling of the community microgrid in grid-connected mode via centralized and distributed optimization is compared in Fig. 6. Taking house #1 for an example, the indoor temperature and the HVAC schedule are shown in Fig. 6a and 6b. As can be seen, by considering building thermal dynamics, the HVAC cooling was switched on around 9 a.m. when the indoor temperature was perfectly 23°C., i.e., the set point. Thus, the house was precooled to avoid or reduce HVAC power consumption during peak price periods (1 p.m. – 2 p.m.), so that the customer's electricity bill would be reduced.

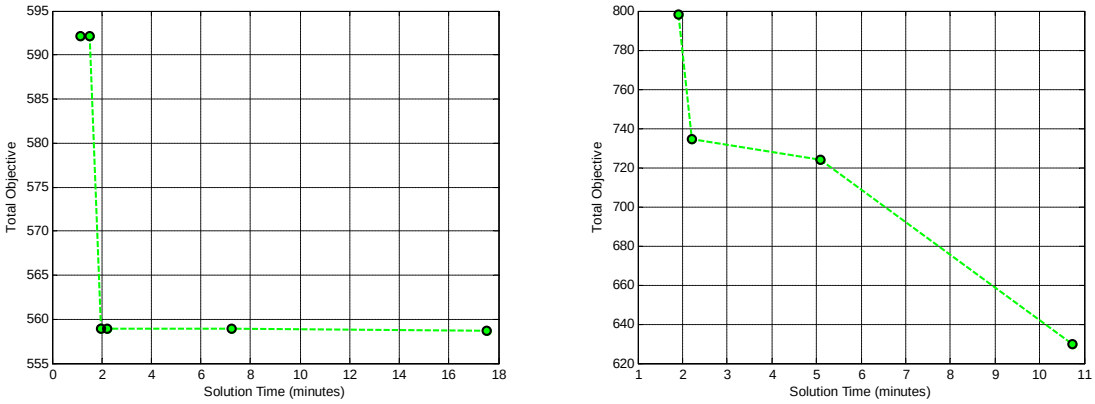

(a) Grid-Connected Mode **(b)** Islanded Mode

Figure 5: Solution time vs. objective value for centralized optimization

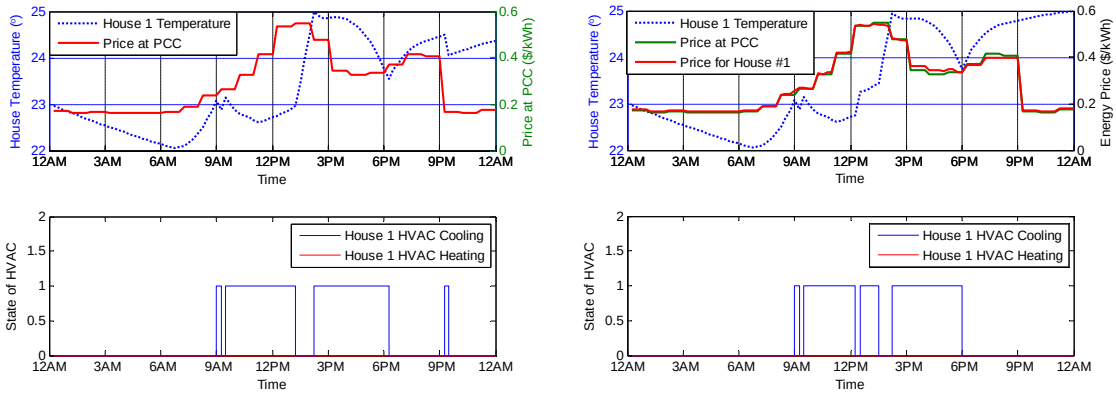

(a) Centralized Optimization **(b)** Distributed Optimization

Figure 6: House temperature and HVAC status in grid-connected mode

Note also that HVAC scheduling by distributed optimization is a little different from scheduling by centralized optimization. This is because the distribution optimization cannot guarantee the global optimum owing to the nonconvexity of the subproblems. Nevertheless, the converged price signal for house #1 generally follows the utility rate at the PCC, as shown in Fig. 6b, since the operating cost dominates the objective function and the PCC can be seen as the marginal units in grid-connected mode. From this point, the utility rate is an excellent candidate for initial price in grid-connected operation.

5.4. Operation in Islanded Mode

The scheduling of the community microgrid in islanded mode via centralized and distributed optimization is compared in Fig. 7. The net demand of the community microgrid, i.e., total load minus PV generation, was calculated and used as an indicator of the electricity price because more expensive DGs needed to be committed in the case of high net demand. In addition, the operating cost dominated the objective function. Thus, net demand reflected the level of electricity prices in general. Still, taking house #1 for an example, the indoor temperature and the HVAC schedule are shown in Fig. 7a and 7b. First, the house was precooled (around 9 a.m.) to reduce HVAC power consumption during high net demand periods in order to reduce customer's costs. Second, both the duration and the value of high-net-demand periods were reduced in the distributed optimization cases. Third, the results of centralized optimization and distributed optimization are slightly different owing to the nonconvexity of the subproblems.

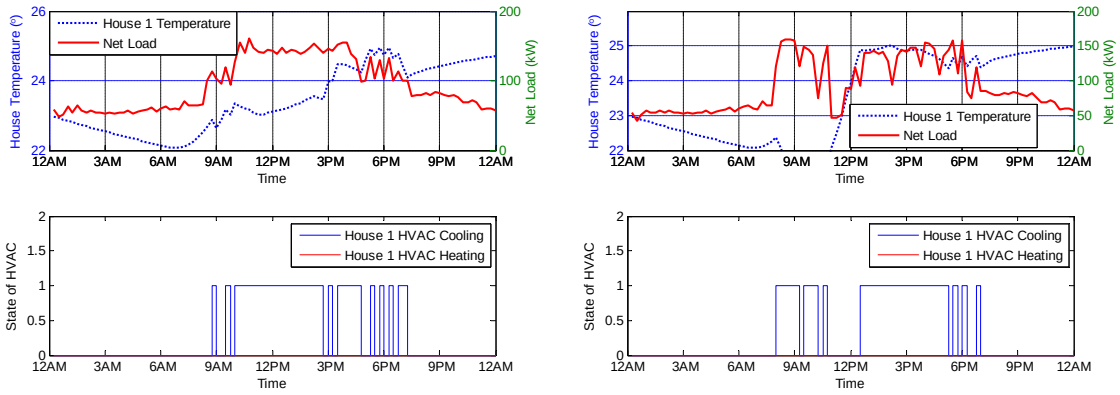

(a) Centralized Optimization **(b)** Distributed Optimization

Figure 7: House temperature and HVAC status in islanded mode

5.5. Convergence of Distributed Energy Management

For the case of distributed optimization, the converged price signals are compared in Fig. 8. In grid-connected mode, as can be seen in Fig. 8a, the price curves of all buses generally follow the price at the PCC. However, there are some differences among the prices for different buses. When the PCC price was low (e.g., 12–7 a.m., 3–5 p.m. and 9–12 p.m.), the power flowed from bus 1 to bus 5 since all DGs are off. The price at bus 5 was the

highest among all the buses because the resulting loss of power transferring from bus 1 to bus 5 was the highest. When the PCC price was high (e.g.,12–2 p.m.), the DGs on bus 3 and bus 4 were committed and the power flowed from bus 3 and 4 to bus 1. The price at bus 1 was the highest. In other words, the electricity price increased along the power flow path. In islanded mode, bus 3 and 4 always had lower prices since all DGs were installed at bus 3 and 4, while bus 2 and 5 had the highest price since it was the end of the power flow path (since bus 1 had no generation or load). Note that the price fluctuated significantly when the load increased or decreased quickly. This is because the rapid increase/decrease in load resulted in the start-up and shutdown of multiple DGs, which involved certain start-up cost.

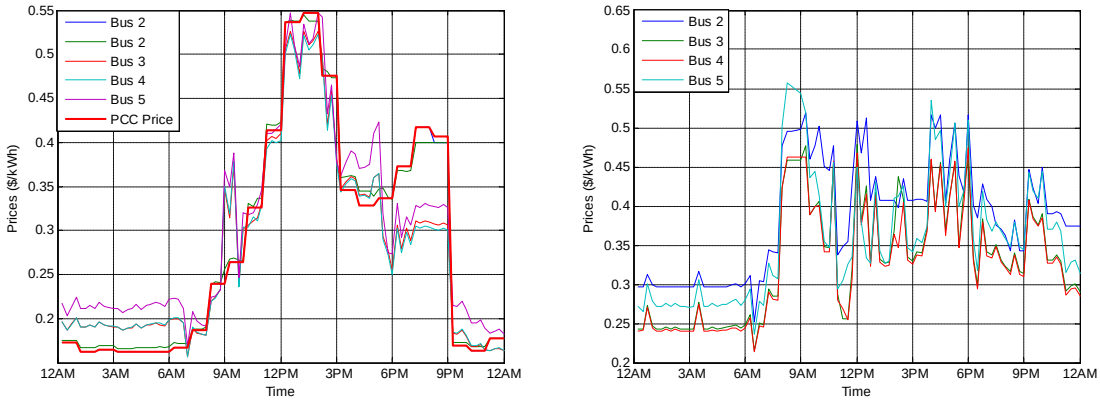

(a) Grid-Connected Mode **(b)** Islanded Mode

Figure 8: Converged price signal λ_{nt} by distributed optimization

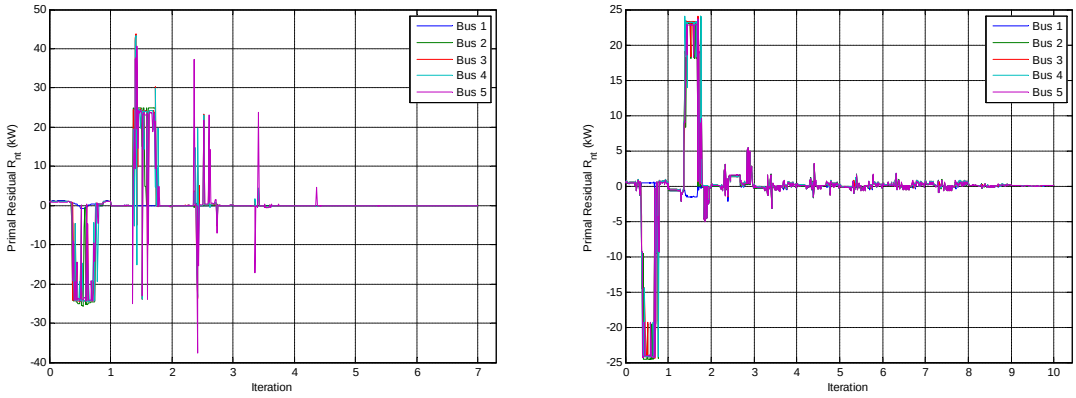

(a) Grid-Connected Mode **(b)** Islanded Mode

Figure 9: Primal residual versus iteration by distributed optimization

For the proposed distributed optimization scheme in both grid-connected and islanded

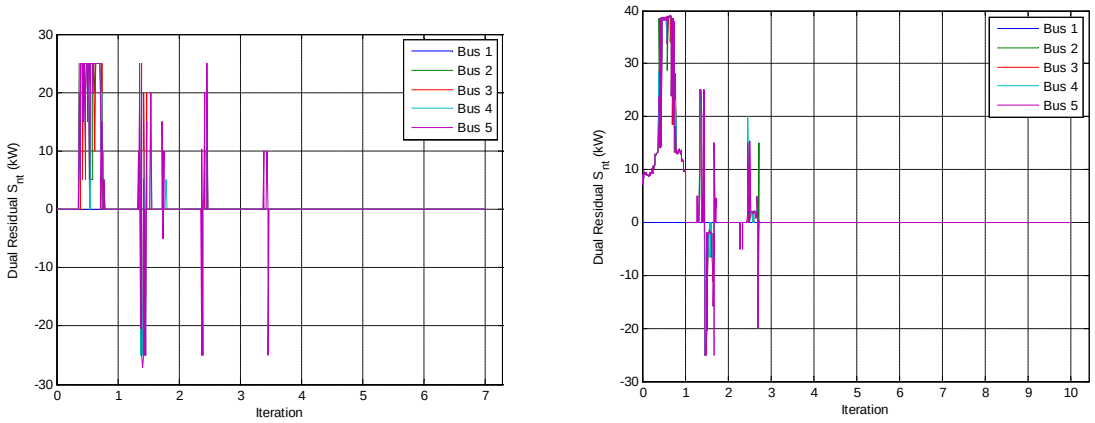

(a) Grid-Connected Mode **(b)** Islanded Mode

Figure 10: Dual residual versus iteration by distributed optimization

modes, a reasonable stopping criterion is that both the primal residual R_{nt} and dual residual S_{nt} must be small, i.e., the power must be balanced at each bus [38]. The primal residual and dual residual are calculated according to equation (39) and (42), and the stopping criterion used is $(R_{nt} \leq 0.5)\,\&\,(S_{nt} \leq 0.5)$. The primal residual and dual residual as a function of the iteration number is shown in Fig. 9 and Fig. 10, respectively. For each iteration, the primal residuals and dual residuals of all time intervals are included and shown in chronological order. As can be seen, the distributed optimization converges quickly. If the algorithm doesn't converge in certain situations, slowly increasing the augmented penalty factor ρ could help reduce the primal residuals and facilitate the convergence.

5.6. 100-house System

To test the scalability of the proposed distributed energy management approach, a 100-house system was constructed based on the 20-house system in Fig. 3. In particular, the houses at each bus were duplicated five times (i.e., there are 25 houses at each bus). Corre-

Table 4: Total objective and solution time of centralized and distributed optimization

Case		Total Objective	Solution Time (Minutes)
Grid-connected	Centralized Optimization	2559.91	144
	Distributed Optimization	2675.02	9
Islanded	Centralized Optimization	3453.52	261
	Distributed Optimization	3614.54	12

spondingly, the sizes of DGs and ESSs were scaled up five times. The loads of each house, system network, and energy price at the PCC were the same. The modified 100-house system should be a representative scale for community microgrids based on the two practical community microgrid projects (62 homes in Alabama Power's Smart Neighborhood Microgrid [43] and 46 townhouses in Georgia Power's Smart Neighborhood Program [44]) and the IEEE European Low Voltage Test Feeder (55 prosumers) [45].

The total objective values and solution times of the centralized optimization and proposed distributed optimization are compared in Table 4. Although the total objective values calculated by distributed optimization are close to those calculated by centralized optimization, the solution times of centralized optimization increase significantly while those of distributed optimization show little change. Therefore, the proposed distributed energy management approach is scalable compared with centralized energy management.

6. Conclusions

This paper proposes a distributed energy management system for community microgrids that considers building thermal dynamics and network operational constraints. On the basis of the price signals and the generation and demand mismatch at each bus, the microgrid central controller and the home energy management system, separately, optimize the scheduling of distributed energy resources and energy storage systems and of the heating, ventilation, and air-conditioning system and other loads The price signals and power imbalance are updated and distributed in each iteration. Thus, customer energy consumption is guided by price signals rather than by direct load control. The distributed energy management model is solved by the alternating direction method of multipliers algorithm. The effectiveness of the proposed model has been validated by the results of numerical simulations.

Although this paper is focused on energy management for microgrids and utility distribution grids, the proposed model can be easily extended to make various ancillary services—such as frequency regulation, spinning and non-spinning reserve, and even virtual inertia provided by customers—transactive. Introducing the proposed distributed energy management approach to power grid management and control architecture can improve the resiliency, reliability and security of the grid and minimize costs and needs for new distribution/transmission capacity, while enabling higher penetration of renewable resources and distributed energy storage. This work paves the way for a future resilient electricity distribution system facilitated by demand-side technologies.

Acknowledgment

This work is supported by the US Department of Energy's Office of Electricity Delivery and Energy Reliability (OE). The authors also would like to thank the support in part by National Natural Science Foundation of China (Grant No. 51877033, 51607033, and 51607034), National Key Research and Development Program of China (2017YFB0903400), Integrated Energy System Innovation Team of Jilin Province (20180519015JH),and International Clear Energy Talent Program (iCET) of China Scholarship Council. This work also made use of Engineering Research Center Shared Facilities supported by the Engineering

Research Center Program of the National Science Foundation and the Department of Energy under National Science Foundation Award Number EEC-1041877 and the CURENT Industry Partnership Program.

References

[1] CERTS Microgrid Concept, 2003, [Online]. Available: http://certs.lbl.gov/certs-der-micro.html.

[2] A. G. Madureira and J. A. Pecas Lopes, "Coordinated voltage support in distribution networks with distributed generation and microgrids," *IET Renew. Power Gen.*, vol. 3, no. 4, pp. 439-454, Dec. 2009.

[3] X. Li, R. Zhang, L. Bai, G. Li, T. Jiang and H. Chen, "Stochastic low-carbon scheduling with carbon capture power plants and coupon-based demand response," *Appl. Energy*, vol. 210, pp. 1219-1228, Jan. 2018

[4] M. Agrawal and A. Mittal, "Micro grid technological activities across the globe: A review," *Int. J. Res. Rev. Appl. Sci.*, vol. 7,no. 2, pp. 147-152, May 2011.

[5] E. Vaahedi, K. Nodehi, D. Heim, F. Rahimi and A. Ipakchi, "The Emerging Transactive Microgrid Controller: Illustrating Its Concept, Functionality, and Business Case," *IEEE Power Energy Mag.*, vol. 15, no. 4, pp. 80-87, Jul. 2017.

[6] W. Gu, Z. Wu, R. Bo, W. Liu, G. Zhou, W. Chen, and A. Wu, "Modeling, planning and optimal energy management of combined cooling, heating and power microgrid: A review," *Int. J. Electr. Power Energy Syst.*, vol. 54, pp. 26-37, Jan. 2014.

[7] B. Belvedere, M. Bianchi, A. Borghetti, C. A. Nucci, M. Paolone, and A. Peretto, "A microcontroller-based power management system for standalone microgrids with hybrid power supply," *IEEE Trans. Sustain. Energy*, vol. 3, no. 3, pp. 422-431, Jul. 2012

[8] G. Cardoso, M. Stadler, A. Siddiqui, C. Marnay, N. DeForest, A. Barbosa-Pvoa, and P. Ferro, "Microgrid reliability modeling and battery scheduling using stochastic linear programming," *Electr. Power Syst. Res.*, vol. 103, pp. 61-69, Oct. 2013

[9] G. Liu, Y. Xu, and K. Tomsovic, "Bidding Strategy for Microgrid in Day-Ahead Market Based on Hybrid Stochastic/Robust Optimization," *IEEE Trans. Smart Grid*, vol. 7, no. 1, pp. 227-237, Jan. 2016

[10] Z. Li, and Y. Xu, "Optimal coordinated energy dispatch of a multi-energy microgrid in grid-connected and islanded modes," *Appl. Energy*, vol. 210, pp. 974-986, Jan. 2018

[11] D. T. Nguyen and L. B. Le, "Optimal Bidding Strategy for Microgrids Considering Renewable Energy and Building Thermal Dynamics," *IEEE Trans. Smart Grid*, vol. 5, no. 4, pp. 1608-1620, Jul. 2014.

[12] S. Mashayekh, M. Stadler, G. Cardoso, and M. Heleno, "A mixed integer linear programming approach for optimal DER portfolio, sizing, and placement in multi-energy microgrids," *Appl. Energy*, vol. 187, pp. 154-168, Feb. 2017

[13] G. Liu, T. Ollis, B. Xiao, X. Zhang and K. Tomsovic, "Community Microgrid Scheduling Considering Network Operational Constraints and Building Thermal Dynamics," *Energies*, vol. 10, pp. 1-19, Oct. 2017.

[14] T. Jiang, Z. Li, X. Jin, H. Chen, X. Li, and Y. M, "Flexible operation of active distribution network using integrated smart buildings with heating, ventilation and air-conditioning systems," *Appl. Energy*, vol. 226, pp. 181-196, Sep. 2018

[15] J. Lavaei, S. Low, "Zero Duality Gap in Optimal Power Flow Problem," *IEEE Trans. Power Syst.,* vol. 27, no. 1, pp. 92-107, Feb. 2012.

[16] M. Farivar and S. Low, "Branch flow model: Relaxations and convexification —Part I," *IEEE Trans. Power Syst.*, vol. 28, no. 3, pp. 2554-2564, Aug. 2013.

[17] Y. Zhang, N. Gatsis, and G. Giannakis, "Robust energy management for microgrids with high-penetration renewables," *IEEE Trans. Sustain. Energy*, vol. 4, no. 4, pp. 944–953, Oct. 2013.

[18] Y. Liu, H. B. Gooi, and H. Xin, "Distributed energy management for the multi-microgrid system based on ADMM," in *Proc. IEEE Power Energy Society General Meeting (PESGM)*, Chicago, IL, Aug. 2017, pp. 1-5.

[19] G. Liu, M. Starke, B. Xiao, X. Zhang and K. Tomsovic, "A New Distributed Optimization for Community Microgrids Scheduling," in *Proc.* 50th Hawaii International Conference on System Sciences (HICSS-50),Waikoloa, HI, Jan. 2017, pp. 3045-3054.

[20] Y. Liang, F. Liu, C. Wang, and S. Mei, "Distributed demand-side energy management scheme in residential smart grids: An ordinal state-based potential game approach," *Appl. Energy*, vol. 206, pp. 991-1008, Nov. 2017.

[21] W. Shi, X. Xie, C. Chu and R. Gadh, "Distributed Optimal Energy Management in Microgrids," *IEEE Trans. Smart Grid*, vol. 6, no. 3, pp. 1137-1146, May 2015.

[22] B. Kim and R. Baldick, "A comparison of distributed optimal power flow algorithms," *IEEE Trans. Power Syst.*, vol. 15, no. 2, pp. 599-604, May 2000.

[23] T. Erseghe, "Distributed optimal power flow using ADMM," *IEEE Trans. Power Syst.*, vol. 29, no. 5, pp. 2370-2380, Sep. 2014.

[24] M. Kraning, E. Chu, J. Lavaei, and S. Boyd, "Dynamic network energy management via proximal message passing," *Foundations and Trends in Optimization*, vol. 1, no. 2, pp. 70-122, 2013.

[25] P. Sulc, S. Backhaus, and M. Chertkov, "Optimal Distributed Control of Reactive Power via the Alternating Direction Method of Multipliers," *IEEE Trans. Energy Conver.*, vol. 29, no. 4, pp. 968-977, Dec. 2014.

[26] W. J. Ma, J. Wang, V. Gupta, and C. Chen, "Distributed energy management for networked microgrids using online ADMM with regret," *IEEE Trans. Smart Grid*, vol. 9, no. 2, pp. 847-856, Mar. 2018.

[27] E. Dall'Anese, H. Zhu, and G. B. Giannakis, "Distributed optimal power flow for smart microgrids," *IEEE Trans. Smart Grid*, vol. 4, no. 3, pp. 1464-1475, Sep. 2013.

[28] M. Bazrafshan and N. Gatsis, "Decentralized Stochastic Optimal Power Flow in Radial Networks With Distributed Generation," *IEEE Trans. Smart Grid*, vol. 8, no. 2, pp. 787-801, Mar. 2017.

[29] P. Scott and S. Thibaux, "Distributed Multi-Period optimal power flow for demand response in microgrids," in *Proc. ACM 6th Int. Conf. Future Energy Syst.*, Bangalore, India, Jul. 2015, pp. 17-26.

[30] M. Khodayar, S. Manshadi, and A. Vafamehr, "The short-term operation of microgrids in a transactive energy architecture," The Electricity Journal, vol. 29, no. 10, pp. 41-48, Dec. 2016.

[31] A. Thavlov, "Dynamic optimization of power consumption," M.S. thesis, Tech. Univ. Denmark, Kongens Lyngby, Denmark, 2008.

[32] P. Bacher and H.Madsen, Identifying suitable models for the heat dynamics of buildings," *Energy Buildings*, vol. 43, no. 7, pp. 15111522, Jul. 2011.

[33] V. Harish and A. Dounis, "Reduced order modeling and parameter identification of a building energy system model through an optimization routine," *Applied Energy*, vol. 162, pp. 1010-1023, Jan. 2016.

[34] T. Saaty, "Decision making-the analytic hierarchy and network processes (AHP/Anp)," J. Syst. Sci. Syst. Eng., vol. 13, pp 1-35, Mar. 2004.

[35] L. Gan, N. Li, U. Topcu, and S. H. Low, "Exact convex relaxation of optimal power flow in radial networks," *IEEE Trans. Autom. Control.*, vol. 60, no. 1, pp. 72–87, Jan. 2015.

[36] M. Baradar, M. R. Hesamzadeh, and M. Ghandhari, "Second-order cone programming for optimal power flow in vsc-type ac-dc grids," *IEEE Trans. Power Syst.*, vol. 28, no. 4, pp. 4282–4291, Nov. 2013.

[37] M. Carrin, and J. M. Arroyo, "A computationally efficient mixed-integer linear formulation for the thermal unit commitment problem," *IEEE Trans. Power Syst.*, vol. 21, no. 3, pp. 1371-1378, Aug. 2006.

[38] S. Boyd, N. Parikh, E. Chu, B. Peleato, E. Eckstein, "Distributed Optimization and Statistical Learning via the Alternating Direction Method of Multipliers" *Foundations and Trends® in Machine Learning,* vol. 3, pp. 1-122, Jan. 2011.

[39] E. Ghadimi, A. Teixeira, I. Shames and M. Johansson, "Optimal Parameter Selection for the Alternating Direction Method of Multipliers (ADMM): Quadratic Problems," *IEEE Trans. Autom. Control*, vol. 60, no. 3, pp. 644-658, Mar. 2015.

[40] M. Hong, Z. Q. Luo, and M. Razaviyayn, "Convergence analysis of alternating direction method of multipliers for a family of nonconvex problems," *SIAM J. Optim.*, vol. 26, no. 1, pp. 337-364, Jan. 2016.

[41] B. Xiao, M. Starke, G. Liu, B. Ollis, P. Irminger, A. Dimitrovski, K. Prabakar, K. Dowling, and Y. Xu, "Development of Hardware-in-the-loop Microgrid Testbed," in *Proc. IEEE Energy Convers. Congr. Expo. (ECCE)*, Montreal, QC, Sep. 2015, pp. 1196-1202.

[42] Oak Ridge National Laboratory (ORNL) Rotating Shadowband Radiometer (RSR). [Online]. Available: http://www.nrel.gov/midc/ornl_rsr/

[43] [Online]. Available: https://www.smart-energy.com/industry-sectors/smart-energy/alabama-powers-smart-neighbourhood/

[44] [Online]. Available: https://www.smartcitiesdive.com/news/atlantas-first-smart-neighborhood-is-under-development/514697/

[45] European Low Voltage Test Feeder, "IEEE PES Distribution Systems Analysis Subcommittee Test Feeders." [Online]. Available: http://ewh.ieee.org/soc/pes/dsacom/testfeeders/